Brazilian Journal of Chemical Engineering
https://doi.org/10.1007/s43153-022-00274-y

ORIGINAL PAPER

Revealing flow structure of air and rice husk in the acrylic suspension furnace: simulation study and cold test experiment

Soen Steven[1] · Elvi Restiawaty[1,2,3] · Pasymi Pasymi[4] · Yazid Bindar[1,2,5]

Received: 15 March 2022 / Revised: 30 July 2022 / Accepted: 26 September 2022

Abstract

An acrylic suspension furnace was used to study the flow structure of air and rice husk. The standard k–ε model with standard wall function was employed in the simulation study while the cold test experiment, for results validation, utilized onionskin (thin oil paper) and rice husk itself. From the simulation, both air and rice husk flows are in swirling mode due to the tangential air. The cold test experiment strengthened that swirl flow of air is indicated by the onionskin movement upward and downward forming a curve and circular directions. On the other hand, swirl flow of rice husk is visualized by the sinusoidal peaks and valleys. In addition, the contribution of secondary air generates recirculation flow at the bottom area of the furnace. Also, there are backflow phenomena that occur, and yet, the revalidation study revealed that modification of tangential air pipes angle with a longer burner length can overcome the problem. Finally, this model can predict the flow structure in a good compliment to the cold test experiment results. Moreover, the less-intensive computation load with a shorter computation time makes it in demand for the design purpose and performance evaluation of process equipment.

Keywords Siliceous ash · Suspension furnace · Cyclone · Swirl · Isotropic turbulent

Introduction

The dependence on massive fossil resources for chemical production and energy generation has been believed to harm humans and the environment (Hernowo et al. 2022a; Sylvia et al. 2019; Ramli et al. 2022; Steven et al. 2022b). This makes the use of biomass, as more renewable resources, increasingly encouraged (Nunes et al. 2014; Wang et al. 2019; Bindar et al. 2022; Hernowo et al. 2022b). One of the abundant biomass in agricultural countries is rice husk (Panuju et al. 2013; Blissett et al. 2017). Its valorization to produce siliceous ash and/or energy could be implemented through combustion in the furnace (Steven et al. 2022d; e). There are several main furnace configurations, i.e. fixed bed, fluidized bed, and suspension furnace (Werther et al. 2000; Fernandes et al. 2016; Blissett et al. 2017; Prasara and Gheewala 2017; Costa and Paranhos 2018).

The fixed bed type is less desirable due to time-consuming and low combustion conversion which is mainly caused by poor air–particle mixing and non-uniform temperature distribution (Werther et al. 2000; Duan et al. 2013; Gomes et al. 2016). On the other hand, the fluidized bed type can remedy the air–particle contact and combustion time. The product is mostly contaminated with the bed material so the cyclone separator installation becomes necessary (Fang et al. 2004; Kuprianov et al. 2010; Suranani and Goli 2012; Nunes et al. 2014). In addition, the suspension furnace is similar to a fluidized bed but does not involve bed material inside (Werther et al. 2000; Fernandes et al. 2016; Blissett et al. 2017). It is well-suitable

✉ Yazid Bindar
ybybyb@fti.itb.ac.id

1 Department of Chemical Engineering, Faculty of Industrial Technology, Institut Teknologi Bandung, Jl. Ganesha 10, Bandung 40132, Indonesia

2 Department of Bioenergy Engineering and Chemurgy, Faculty of Industrial Technology, Institut Teknologi Bandung, Jl. Ganesha 10, Bandung 40132, Indonesia

3 Research Group on Design and Development of Chemical Engineering Processes, Faculty of Industrial Technology, Institut Teknologi Bandung, Jl. Ganesha 10, Bandung 40132, Indonesia

4 Department of Chemical Engineering, Faculty of Industrial Technology, Bung Hatta University, Padang 25173, Indonesia

5 Research Group on Biomass and Food Processing Technology, Faculty of Industrial Technology, Institut Teknologi Bandung, Jl. Ganesha 10, Bandung 40132, Indonesia

for biomass with low moisture content, it has no bed material contamination, and a cyclone is usually installed to capture the elutriated particle (Kapur et al. 1984; Werther et al. 2000).

The application of rice husk combustion in an appropriate furnace geometry to provide excellent mixing should consider the design improvement and combustion techniques (Singh et al. 2013; Blissett et al. 2017; Steven et al. 2022f). Perfect rice husk combustion is expected to generate maximum thermal energy (Steven et al. 2022d) as well as ash with high silica and low unburnt carbon content (Steven et al. 2021). A study on rice husk combustion simulation through computational fluid dynamics (CFD) in fluidized bed combustor exhibited that recirculating zone prolongs the particle trajectory and residence time by returning them to the furnace (Rozainee et al. 2010). Another CFD study on biomass and coal co-firing in a tangential furnace resulted in a number of unburned particles and providing a minor redesign of the air supply technique was strongly suggested (Bhuiyan and Naser 2015).

A simulation study of torrefied biomass co-firing in a pulverized-fired combustor still faced poor efficiency because of incomplete biomass decomposition due to coarser particles (Stroh et al. 2015). All the preceding studies imply that the air–particle hydrodynamics should be understood first to achieve complete combustion. The air–particle hydrodynamics plays an important role in the bubbling fluidized bed reactor performance to model the particle movement and collision accurately (Cardoso et al. 2019; Yang et al. 2019). The air and particle (Mischantus) hydrodynamics study in a biomass cyclonic burner showed a meaningless result discrepancy between simulation and experiment (Pasymi et al. 2020a, b).

To date, there is still lacking a comprehensive understanding of rice husk hydrodynamics aspects (Singh et al. 2013; Guan et al. 2014; Li et al. 2019; Yang et al. 2020), especially in the suspension furnace. In order to prevent an excessive trial error that results in massive expenditure in design, a CFD study should be carried out at first, and further, the results are validated (Pasymi et al. 2020b; Steven et al. 2022a). So far, the validation is mostly using laser Doppler anemometry or particle image velocimetry which are cost-intensive (Hoekstra et al. 1999; Nemoda et al. 2005; Pashtrapanska et al. 2006; Panneerselvam et al. 2009).

The flow structure of air and rice husk under the attendance of tangential air and secondary air in the acrylic suspension furnace was thus investigated in this study by simulation through CFD. The result is then validated with cheap and simple cold test experiment. There were five locations to be investigated: two of them are located in the burner and the rest are located in the main furnace. The observed variables were air pathline and rice husk particle track.

Methodology

Geometry and simulation condition

The acrylic suspension furnace has three parts, i.e. main furnace, burner, and cyclone. The geometry of the main furnace is a cylinder with 300 mm in diameter and 1970 mm in height. The bottom area of the furnace has a conical geometry with 218 mm of height. In this area, there are two lower secondary air pipes with a diameter of 50 mm and has 60° angle from the conical slant surface. There are another two upper secondary pipes at the location 400 mm from the top furnace with the inclination with respect to the vertical position being 30°.

The furnace has one burner on the left and one burner on the right. Burners are located at 695 mm from the bottom furnace with 130 mm in diameter and 1620 mm in length. Each burner is connected with an axial blower at the end position and two tangential air pipes at the position of about 350 mm from the end of the burner. Tangential air pipe has a rectangular geometry with 250 mm of length, 50 mm of width, 30 mm of depth, and 75° inclined from the horizontal burner position. The rice husk feeder position is at 210 mm from the end of each burner and has a cylindrical shape with 100 mm in diameter, 100 mm in height, and sinks 30 mm into the burner surface.

The furnace outlet position has 150 mm of pipe height and is directly connected with a cyclone separator with a cylinder height of 500 mm and a cone height of 750 mm. Cyclone has a body diameter of 200 mm, ash collector diameter of 50 mm, vortex finder diameter of 100 mm, and vortex finder height of 200 mm. The detailed dimension of the acrylic suspension furnace can be seen in the Supplementary File.

Rice husk with a density of 661.92 kg/m^3 was fed into the furnace through the feeder. The particle size distribution follows Rosin–Rammler from 2 to 8 mm with a mean diameter of 2.5 mm and sphericity factor (φ_p) of 0.5. The particle–wall reflection coefficient was 1. Air was blown with the amount in such a way that air to rice husk ratio is 10.7 (Steven et al. 2022d). The physical properties of air were inputted at 25 °C. The air supply was distributed into two axial air (25%), four tangential air (45%), two lower secondary air (8.4%), and two upper secondary air (21.6%). The turbulent viscosity ratio for all boundary conditions was set at 10%. After simulation, the pathline profile for air flow structure and particle track profile for rice husk flow structure was

extracted. Also, the amount of particle loss was also evaluated in the simulation and cold test experiment.

CFD model

The standard k–ε model was applied in this study. It was derived from Reynolds-Averaged Navier–Stokes (RANS) equation which calculated the static pressure (p) and velocities in three-dimensional directions as a time-averaged result (Malik et al. 2010; Norton et al. 2013; Malekjani and Jafari 2018). Meanwhile, the standard wall function was employed to evaluate the condition near the wall since it is widely used in industrial applications (ANSYS 2019). The mathematical model for fluid flow is using Eulerian approach. It consists of mass conservation that follows Eq. 1 and momentum conservation in three-dimensional directions which are given in Eq. 2.

Turbulent viscosity (μ_t) is an important contribution to turbulent flow modelling where the value is then described in the forms of turbulent kinetic energy (k) and turbulent kinetic dissipation rate (ε) terms (Bindar 2017; ANSYS 2019; Steven et al. 2022a), as seen in Eq. 3. Subsequently, k is specifically described in Eq. 4 whereas Eq. 5 is for determining ε.

$$\frac{\partial \rho}{\partial t} + \sum_{i=x}^{y,z} \frac{\partial \left(\rho \overline{u_i}\right)}{\partial i} = 0 \tag{1}$$

$$\rho \frac{\partial \overline{u_x}}{\partial t} + \sum_{i=x}^{y,z} \left[\overline{u_i} \frac{\partial \left(\rho \overline{u_x}\right)}{\partial i} \right] = -\frac{\partial \overline{p}}{\partial x} + \sum_{i=x}^{y,z} \left\{ \frac{\partial}{\partial i} \left[\left(\mu + \mu_t\right) \frac{\partial \left(\rho \overline{u_x}\right)}{\partial i} \right] \right\} + \rho g_x + F_{e,x} \tag{2a}$$

$$\rho \frac{\partial \overline{u_y}}{\partial t} + \sum_{i=x}^{y,z} \left[\overline{u_i} \frac{\partial \left(\rho \overline{u_y}\right)}{\partial i} \right] = -\frac{\partial \overline{p}}{\partial y} + \sum_{i=x}^{y,z} \left\{ \frac{\partial}{\partial i} \left[\left(\mu + \mu_t\right) \frac{\partial \left(\rho \overline{u_y}\right)}{\partial i} \right] \right\} + \rho g_y + F_{e,y} \tag{2b}$$

$$\rho \frac{\partial \overline{u_z}}{\partial t} + \sum_{i=x}^{y,z} \left[\overline{u_i} \frac{\partial \left(\rho \overline{u_z}\right)}{\partial i} \right] = -\frac{\partial \overline{p}}{\partial z} + \sum_{i=x}^{y,z} \left\{ \frac{\partial}{\partial i} \left[\left(\mu + \mu_t\right) \frac{\partial \left(\rho \overline{u_z}\right)}{\partial i} \right] \right\} + \rho g_z + F_{e,z} \tag{2c}$$

$$\mu_t = 0.09 \rho \frac{k^2}{\varepsilon} \tag{3}$$

$$\rho \frac{\partial k}{\partial t} + \sum_{i=x}^{y,z} \left[\overline{u_i} \frac{\partial (\rho k)}{\partial i} \right] = \sum_{i=x}^{y,z} \left\{ \frac{\partial}{\partial i} \left[\left(\mu + \frac{\mu_t}{1.0}\right) \frac{\partial k}{\partial i} \right] \right\} + G_k - Y_k \tag{4a}$$

$$G_k = 2\mu_t \sum_{i=x}^{y,z} \left[\left(\frac{\partial \overline{u_i}}{\partial i} \right)^2 \right] + \mu_t \sum_{i=x}^{y,z} \sum_{j=y}^{z,x} \left[\left(\frac{\partial \overline{u_i}}{\partial j} + \frac{\partial \overline{u_j}}{\partial i} \right)^2 \right] \tag{4b}$$

$$Y_k = \rho \varepsilon \tag{4c}$$

$$\rho \frac{\partial \varepsilon}{\partial t} + \sum_{i=x}^{y,z} \left[\overline{u_i} \frac{\partial (\rho \varepsilon)}{\partial i} \right] = \sum_{i=x}^{y,z} \left\{ \frac{\partial}{\partial i} \left[\left(\mu + \frac{\mu_t}{1.3}\right) \frac{\partial \varepsilon}{\partial i} \right] \right\} + 1.44 \frac{\varepsilon}{k} G_k - 1.92 \rho \frac{\varepsilon^2}{k} \tag{5}$$

where ρ is air density, μ is air viscosity, g is gravity acceleration constant, and F_e is the external body forces per fluid volume unit that arise from interaction with the dispersed phase (ANSYS 2019).

In the meantime, the particle movement caused by fluid flow is defined by a discrete phase model which utilizes the Eulerian-Langrangian approach (ANSYS 2019; Nakhaei et al. 2020; Steven et al. 2022a). The particle velocity field is influenced by the momentum balance of each particle and is presumed no interaction within particles (inert), so it only interacts with the fluid through particle–fluid drag force which is formulated by a drag equation (Bindar 2017; Park and Choi 2019). The used empirical equation for drag coefficient (C_D) is written in Eq. 6 (Haider and Levenspiel 1989). For every particle which has density ρ_p, diameter d_p and sphericity factor φ_p, the particle velocity field has components of $\overline{u_{px}}$, $\overline{u_{py}}$, and $\overline{u_{pz}}$. The particle momentum conservation equation is expressed in Eq. 7.

$$C_D = \frac{\beta_1 Re_{p,i}}{\beta_2 + Re_{p,i}} + \frac{24}{Re_{p,i}} \left(1 + \beta_3 Re_{p,i}^{\beta_4}\right) \tag{6a}$$

$$Re_{p,i} = \frac{\rho d_p \left(\overline{u_i} - \overline{u_{pi}}\right)}{\mu} \tag{6b}$$

$$\begin{aligned} \beta_1 &= \exp\left(4.905 - 13.894\varphi_p + 18.422\varphi_p^2 - 10.260\varphi_p^3\right) \\ \beta_2 &= \exp\left(1.468 + 12.258\varphi_p - 20.732\varphi_p^2 + 15.885\varphi_p^3\right) \\ \beta_3 &= \exp\left(2.329 - 6.458\varphi_p + 2.449\varphi_p^2\right) \\ \beta_4 &= 0.096 + 0.556\varphi_p \end{aligned} \tag{6c}$$

$$\frac{\partial \overline{u_{pi}}}{\partial t} = \left(\overline{u_i} - \overline{u_{pi}}\right) \left(\frac{3\mu C_D Re_{p,i}}{4\rho_p d_p^2} \right) + \frac{\rho_p - \rho}{\rho_p} g_i + F_{a,i} \rightarrow i = x, y, and z \tag{7}$$

where $F_{a,i}$ is an additional acceleration force per particle mass unit term (ANSYS 2019).

Numerical solution setup

The aforementioned problem was numerically solved using a commercial CFD software package, ANSYS Fluent 2021 v.20. The simulation was undergone under an optimal grid cell of 1,950,000 (Steven et al. 2022a). The pressure-based steady-state solving method uses a coupled algorithm for pressure–velocity coupling. The spatial discretization methods are outlined in Table 1 and the pseudo-transient explicit relaxation factors were taken from ANSYS default value: 0.5 for pressure, 0.5 for momentum, 1 for density, 1 for body forces, 0.75 for turbulent kinetic energy, 0.75 for turbulent dissipation rate, and 1 for turbulent viscosity. In this procedure, the residual error absolute criteria were set at 10^{-6} to guarantee convergence. The pseudo-transient calculation with an automatic time-step method and time scale factor 1 was performed for 2000 iterations.

Cold test experiment procedure

The acrylic suspension furnace was constructed with clear and translucent acrylic material in order to facilitate the flow structure visualization. The furnace geometry was fabricated part per part and each part was supplemented with flanges. The black rubbery gasket was installed between flanges and connected using bolts that clamped with nuts. The gasket providence is purposed to prevent acrylic break propagation caused by high mechanical stress from bolts and vibration stress from the blower as well as to prevent air leakage (Mohammed et al. 2018). Afterward, the furnace and blower frames were constructed to erect the furnace and support the blower position. In absence of a frame, there is a high probability of acrylic cracking due to the blower mass. The whole frame was made of cold-formed steel and the joints were locked with a threaded steel bolt. The furnace with the frame is shown in Fig. 1a.

The experiment was carried out for two objects: air and particle. For air flow structure visualization, onionskin (thin oil paper) with 100 mm length and 5 mm width was embedded on a string with a distance for each paper of 5 mm. The string was then clung in five locations test as presented in Fig. 1b. For particle flow structure visualization, rice husk was fed into the feeder and was blown by the air with the aforementioned air proportion. All the visualized results were captured by the camera.

Table 1 Spatial discretization solving methods

Parameter	Method
Gradient	Least square cell-based
Pressure	Second order
Momentum	Second order upwind
Turbulent kinetic energy	First order upwind
Turbulent dissipation rate	First order upwind

Results and discussion

Air flow structure in the suspension furnace

A cold test experiment is an important tool for simulation result validation and aims to visualize in which direction the onionskin will wave under the effect of axial and/or tangential air. It was first done at left and right burner locations. For conditions with no air was supplied, all of the onionskin is in the stationary state with a downward direction, Figs. 2a and 3a. When only an axial blower was applied, the onionskin wave uniformly in the same direction along with the axial air flow. For both left and right burners under influence of axial air, the flow structure obtained from the simulation is in good agreement with the experiment as served in Figs. 2b, c and 3b, c.

The next experiment was performed with the attendance of axial and tangential air flows in the burner. Tangential air supply can generate swirl flow and it was proven through the onionskin movement direction. The movement shows a wavy pattern in the axial direction, in the curve direction, and circularly moves upward and downward as depicted in Fig. 2d, e for the left burner and Fig. 3d–g for the right burner. The air flow structure in the left and right burners under the presence of axial and tangential air from the simulation predictions are all qualitatively reasonable with the results obtained from the experiment.

Subsequently, the cold test experiment was conducted on the bottom, middle, and top areas of the furnace, and the results are presented in Fig. 4. In this condition, all blowers (axial, tangential, and secondary) were turned on and the onionskin movement direction was scrutinized in detail. For the bottom area of the furnace, the flow swirled because of the turbulence near the lower secondary air supply. When getting further from the lower secondary air, the swirl intensity becomes weaker and it is proven by the onionskin movement pattern in the middle and top area of the furnace. As the figure implies, again, there is relatively a small gap in the air flow structure between the predicted result from the simulation and the visualization from the cold test experiment.

Rice husk flow structure in the suspension furnace

Besides validating the air flow structure, the cold test experiment was also implemented to validate and visualize the rice husk flow structure. By design, this furnace has two rice

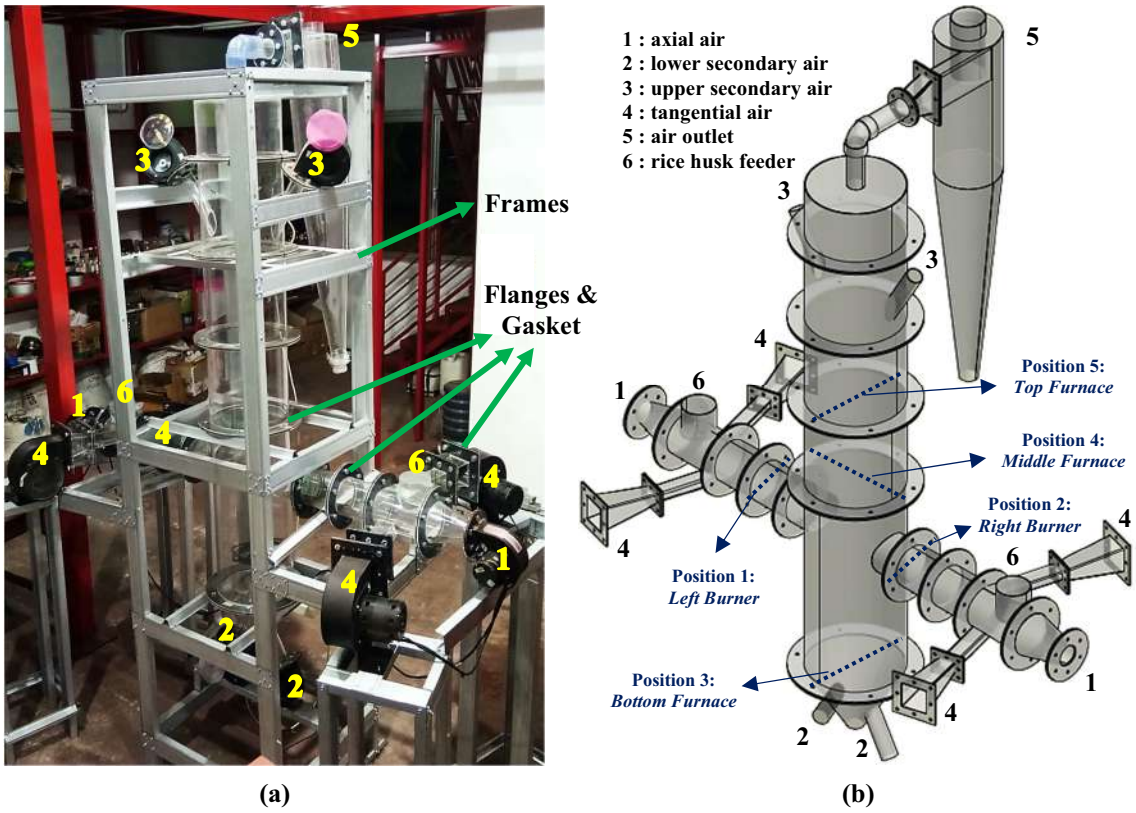

Fig. 1 Acrylic suspension furnace (**a**); five locations test for air flow structure visualization (**b**)

husk feeders which are located on left and right burners. This makes continuous feeding becomes difficult and quite impossible to be operated. To overcome this matter, as much as 575 g of rice husk was fed in batch mode with each burner occupying ½ of the total rice husk load. In such a way, rice husk was arranged to produce a low void fraction before axial and secondary air blowers were turned on. According to the simulation and experiment, rice husk flows in the axial direction in dominance before they enter the furnace and flow downward caused of gravity as seen in Fig. 5a, b. Nevertheless, there is a slight difference in the simulation profile that rice husk has a weak sinusoidal pattern which is strongly believed due to the reflection with the burner wall. In the simulation, the reflection coefficient was set at 1 and this is indeed dissimilar to the actual particle–wall reflection condition.

The final experiment involved all blowers to determine the effects of tangential and secondary air on the rice husk flow structure. Tangential air providing compels the rice husk particle to flow along the burner wall and consequently creates the swirl pattern in dominance compare to the particle–wall reflection (Pasymi et al. 2020b). The two-dimensional swirl pattern mapping is figured out as a sinusoidal wave with peaks and valleys. Under the same rice husk load and air flowrate, the swirl amount was recorded in a varying range from 1 to 3. The varying swirl amount happens because the process still has not yet reached a fully steady-state condition as the simulation does. At the beginning of the process, the swirl pattern is recorded to have 1 peak and 2 valleys as captured in Fig. 5c, d. Apart from that, under more steady-state conditions, the swirl pattern consists of 2 peaks and 3 valleys on the left burner as well as 3 peaks and 3 valleys on the right burner, as given in Fig. 5e–h.

When rice husk flow arrives at the end of the burner position, it will continue to flow downwards to the bottom of the furnace (Kapur et al. 1984). As a consequence of the secondary air supply, rice husk undergoes recirculation flow in the area between the bottom and middle furnace (Steven et al. 2022a), as seen in Fig. 5g. The recirculation plays an important role to extend the particle residence time and hence maximize the air–particle contact (Lin

Fig. 2 Air flow structure in the left burner

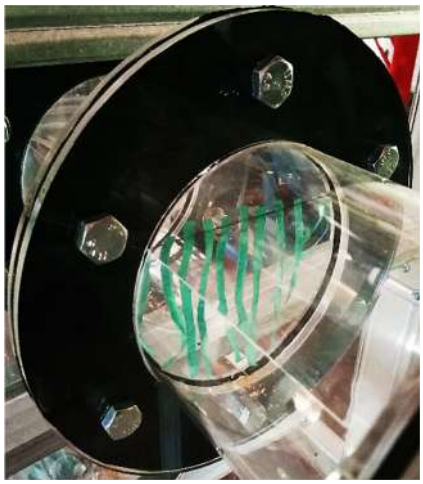

(a)

No air was supplied

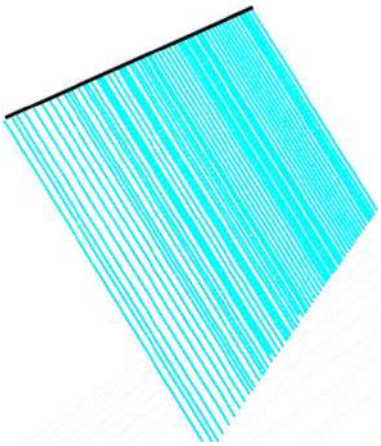

(b)

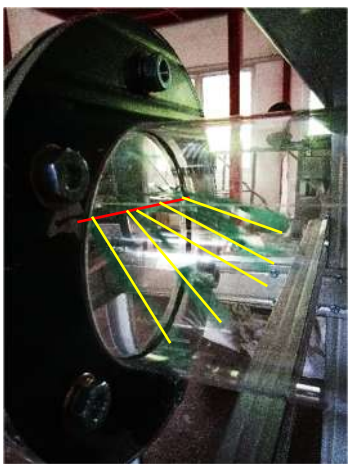

(c)

Only axial air was supplied (b: simulation; c: experiment)

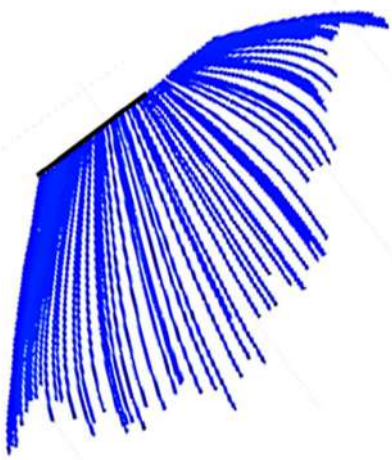

(d)

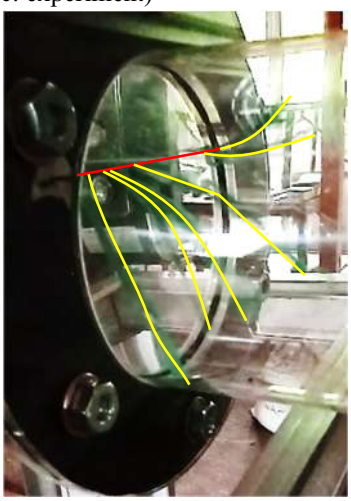

(e)

Axial air and tangential air were supplied (d: simulation; e: experiment)

Fig. 3 Air flow structure in the right burner

(a)

No air was supplied

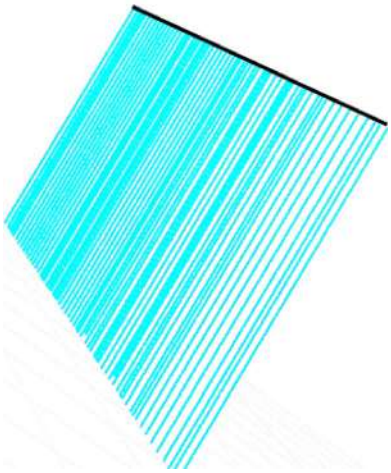

(b)

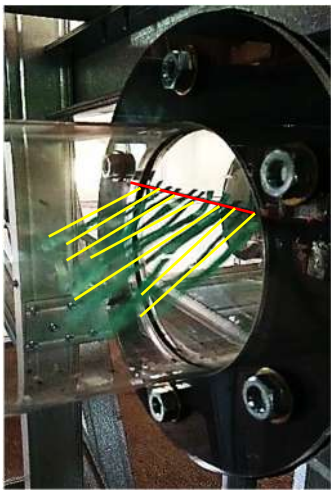

(c)

Only axial air was supplied (b: simulation; c: experiment)

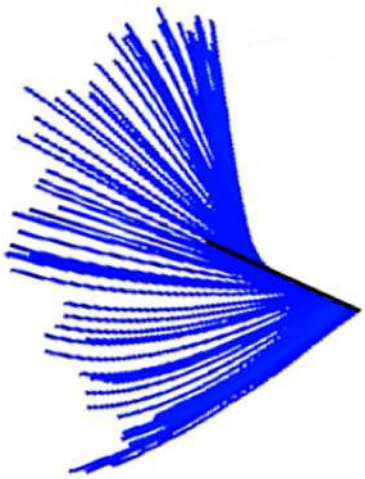

(d)

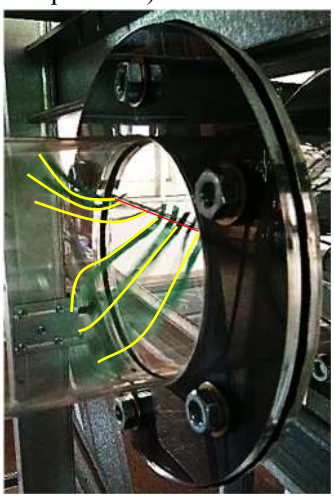

(e)

Axial air and tangential air were supplied (d: simulation; e: experiment)

Fig. 3 (continued)

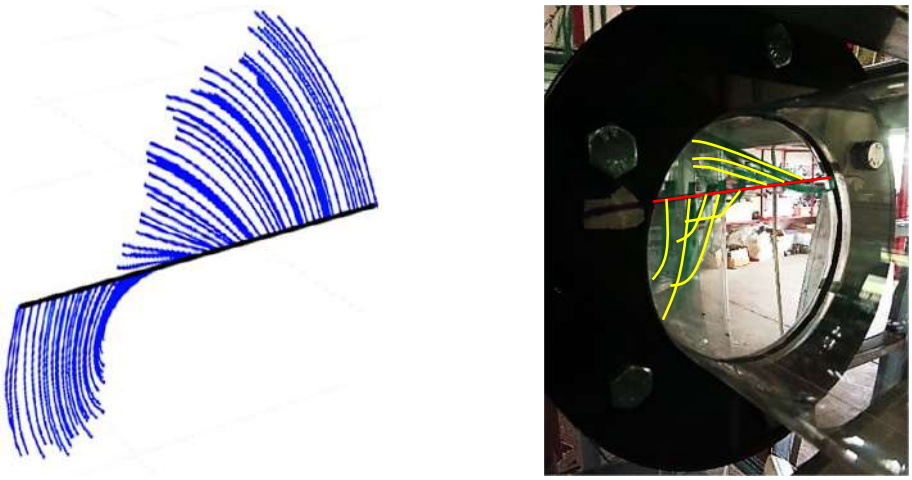

(f) **(g)**

Axial air and tangential air were supplied (f: simulation; g: experiment)

et al. 1997; Koksal 2001; Chokphoemphun et al. 2019). For a long time, rice husk will settle in the bottom area of the furnace to be collected later. Although the suspension burner produces a great deal of airborne ash (Kapur et al. 1984), interestingly this study found only 1.4 g of a fine particle of rice husk was flown to the top area of the furnace and entered the cyclone. This finding is strengthened by the statement that a fine particle with a diameter of less than 1 mm tends to be blown out and captured in the cyclone (Rozainee 2007). The escaped particle from the cold test experiment is 0.23% which is far lower than the simulation predicts, 11.06%.

The model performance for predicting air and particle flow structure

For most of the part, the standard k–ε model has a good performance to predict high Reynold flow or fully turbulent regime (Bindar 2017; ANSYS 2019). Unfortunately, the performance becomes frail when predicting complex flow with rotations, vortices, and intense swirls (Hoekstra 2000; Nemoda et al. 2005; Huang et al. 2010; Pasymi et al. 2017, 2020a; Gao et al. 2018). Following the previous results, interestingly, the air flow structure obtained from the simulation has an adequate consistency with the experiment. Referring to the five locations test, the standard k–ε model is still able to predict the flow behavior with a tolerable difference between simulation and experiment, especially for the location in the top area of the furnace. This is might be induced by standard k–ε model which assumes that velocity fluctuation in all directions is equal, known as isotropic turbulent flow (Khosravi Nikou and Ehsani 2008; ANSYS 2019). Meanwhile, in reality, the flow is anisotropic where the fluctuation behavior is complex and caused by the different fluctuation component values in each direction (Khosravi Nikou and Ehsani 2008; Bindar 2017; Malekjani and Jafari 2018; Steven et al. 2022a). Nevertheless, this model has already shown its ability and versatility to give a logical result in predicting fairly intense swirl flow behavior with a large Reynold Number ($Re = 65{,}000$).

Apart from that, the particle trajectories modelling with Eulerian–Lagrangian approach is actually proper for dilute particle concentration (Singh et al. 2013; Nakhaei et al. 2020). In line with the result from this study, there is a slight discrepancy in particle flow structure which is strongly caused by the distinction of inputted rice husk intrinsic parameter between simulation and actual condition. It cannot be denied that rice husk particle size and sphericity factor are the two most difficult intrinsic parameters to be determined accurately (Pasymi et al. 2020b). The assumption of particle rotational flow negligence also leads to the flow structure difference.

This study, however, reveals that the standard k–ε model associated with discrete phase model still has the capability to predict the flow structures with a slight discrepancy in the result between simulation and experiment. Furthermore, the standard k–ε model is categorized as the simplest two-equation model so that it consumes the lowest computational load, as well as fastest computational time, compared to the

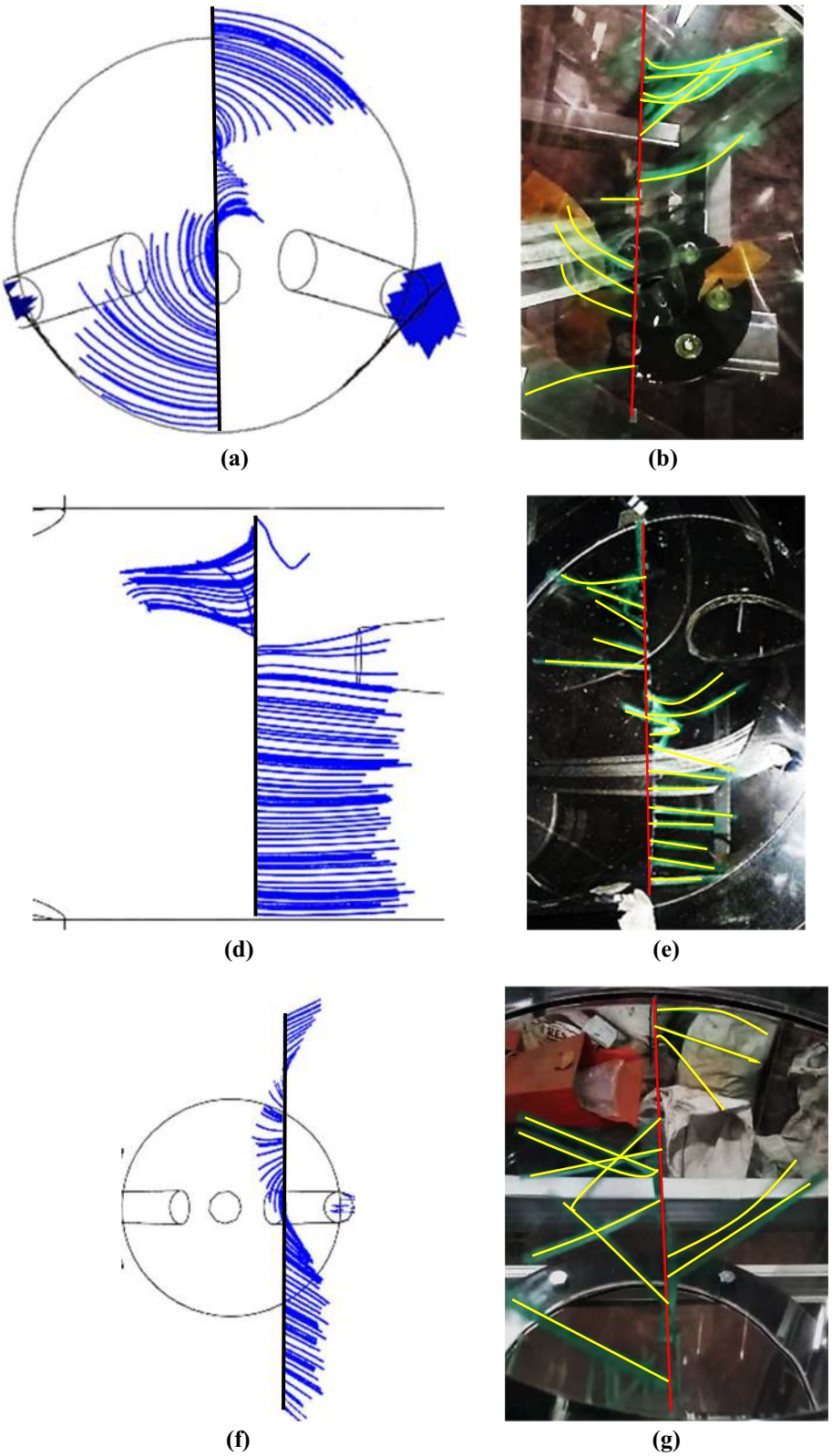

Fig. 4 Air flow structure in the acrylic suspension furnace at bottom area (**a**, **b**), middle area (**c**, **d**), dan top area (**e**, **f**)

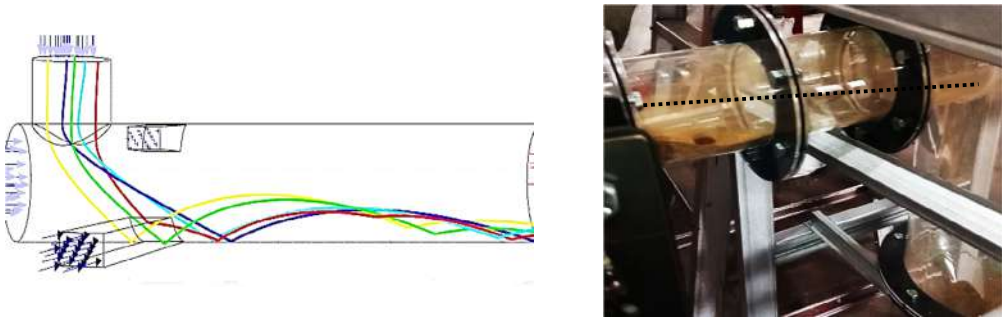

(a) **(b)**

Axial air and secondary air were supplied (a: simulation; b: experiment)

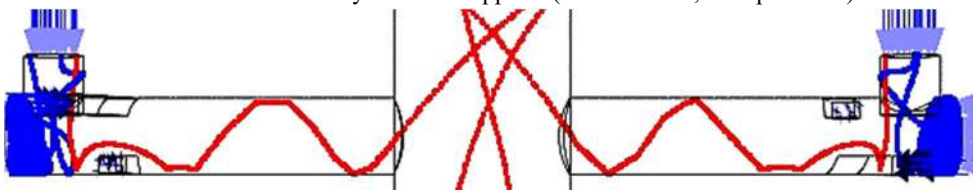

(c)

All air were supplied, simulation

(d)

All air were supplied, experiment

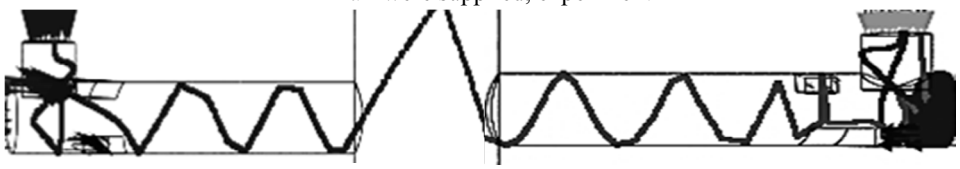

(e)

All air were supplied, simulation

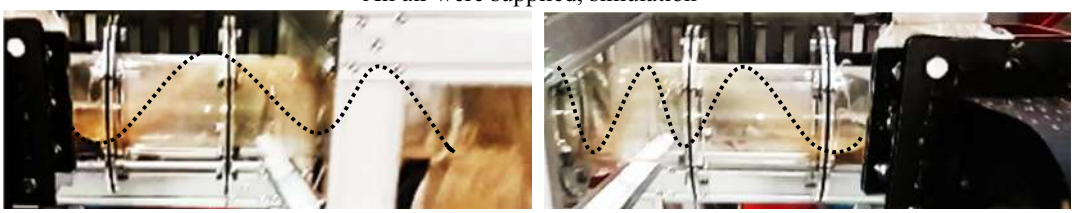

(f)

All air were supplied, experiment

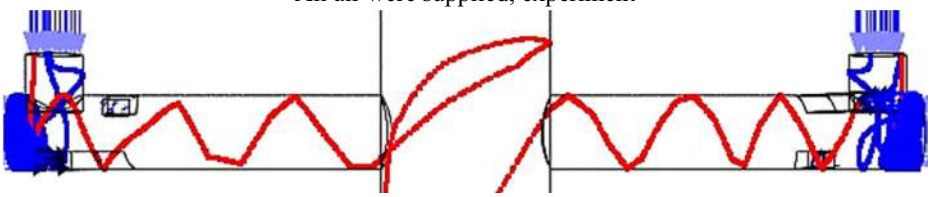

(g)

All air were supplied, simulation

Fig. 5 Rice husk flow structure in the acrylic suspension furnace

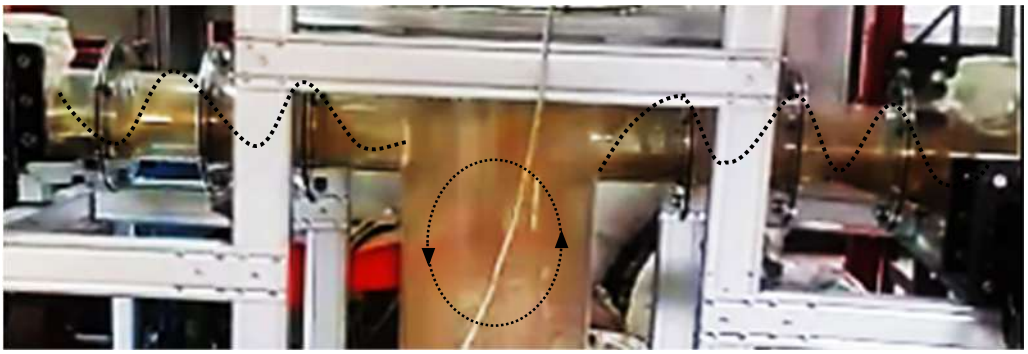

(h)
All air were supplied, experiment

Fig. 5 (continued)

other turbulent models (Defraeye 2014). As a consequence, it is very useful and in-demand to design and evaluate the performance of process equipment.

Attendance of backflow phenomenon: revalidation from experiment to simulation

The backflow phenomenon frequently occurs in the cold test experiment for rice husk flow structure. Actually, rice husk should flow in a direction corresponding to air flow direction, that is away from the axial blower. The particle backflow, hence, is mainly caused by the air backflow that brings the rice husk back to the axial blower. The rice husk backflow phenomenon is captured in Fig. 6. Due to this phenomenon, the revalidation study from experiment to simulation was then carried out.

At first, this furnace has tangential air pipes of 75° for it could create intense and high turbulence as well as longer particle residence time (Steven et al. 2022g). However, the emergence of the backflow phenomenon leads to the need for modifications made from the simulation study. It turns out that the simulation observes an air flow collision between upper and lower tangential air for tangential air pipes of 75°. This condition creates air split to flow back into the axial blower and leads to intense backflow both for air flow (Fig. 7a) and rice husk flow (Fig. 7b).

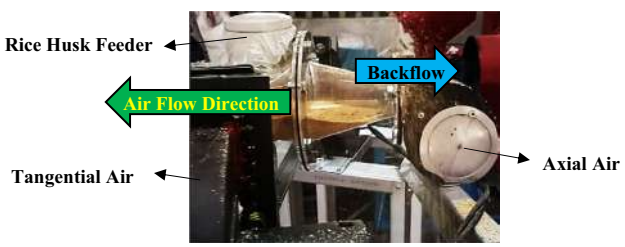

Fig. 6 Backflow phenomenon in the cold test experiment

On the other hand, the backflow intensity weakens when tangential air pipes of 60° (Fig. 8a, b) and become in absence of air backflow for tangential air pipes of 45° (Fig. 9a). Under tangential air pipes of 45°, the rice husk flow structure is also in absence of backflow, as strengthened in Fig. 9b. The suspension furnace with tangential air pipes of 45° is now proposed to be chosen because of the proper criteria to avoid particle backflow phenomenon. Contrary, the tangential air pipes of 45° could lessen the air–particle intense contact but providing a longer burner is recommended to overcome this contradictive problem (Steven et al. 2022c). Therefore, the suspension furnace with a longer burner and tangential air pipes of 45° is expected to produce intense air–particle flow with no backflow phenomenon.

Conclusions

The flow structure of air and rice husk under axial, tangential, and secondary air in the acrylic suspension furnace have been studied in detail through CFD and cold test experiment. Based on the study, the tangential air supply is proven to generate swirl flow patterns for both air and rice husk. Air swirl flow is indicated by the onion-skin movement in a curve direction and circularly moves upward and downward. For rice husk flow structure, the swirl flow is reflected by the generation of sinusoidal peaks and valleys in the burner. Additionally, the secondary air creates recirculation flow before rice husks fall to the bottom of the furnace. There is also a backflow phenomenon that is recorded in the rice husk flow structure due to the flow collision of lower and upper tangential air. From the revalidation study, modification of tangential air pipes, as well as longer burner length, can create intense air–particle contact without backflow. Conclusively, the standard k–ε model can predict the flow structure with an accurate performance as well as low computation load

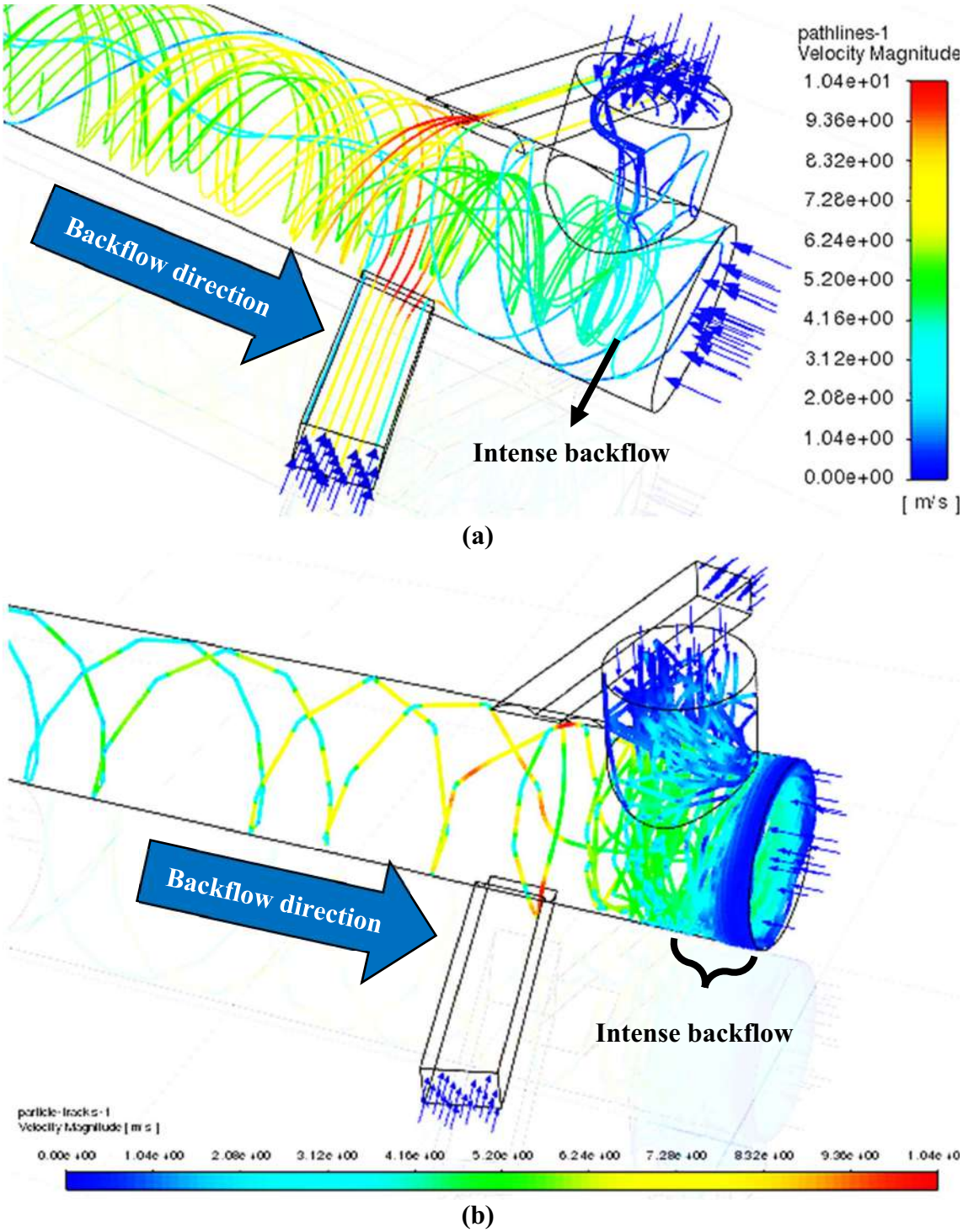

Fig. 7 Backflow investigation at tangential air pipe of 75° for air flow (**a**), dan rice husk flow (**b**)

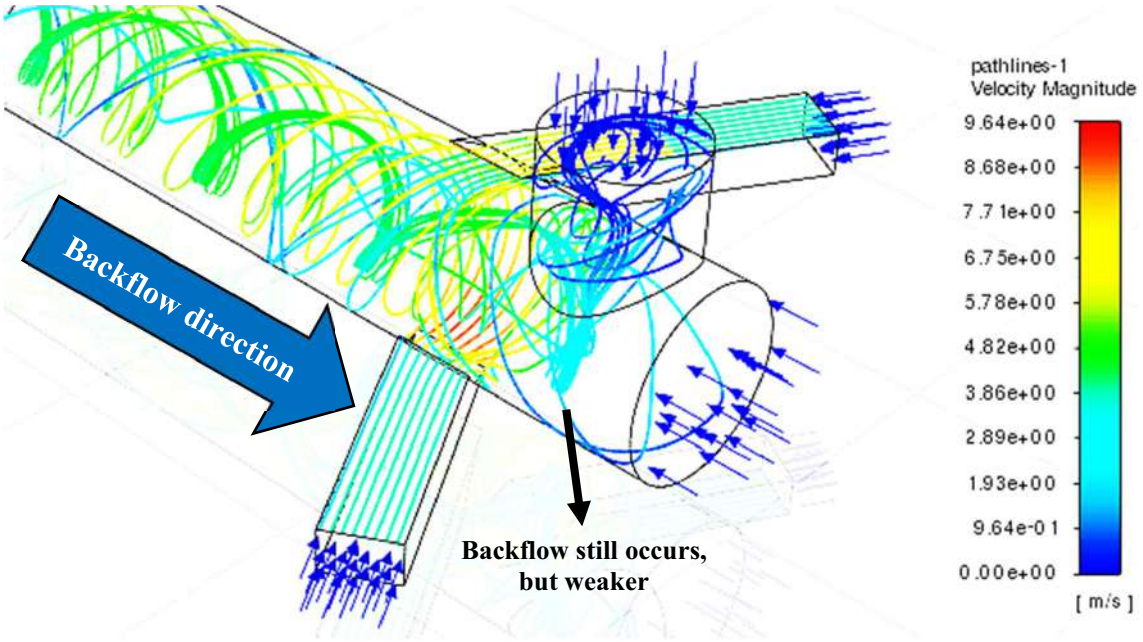

(a)

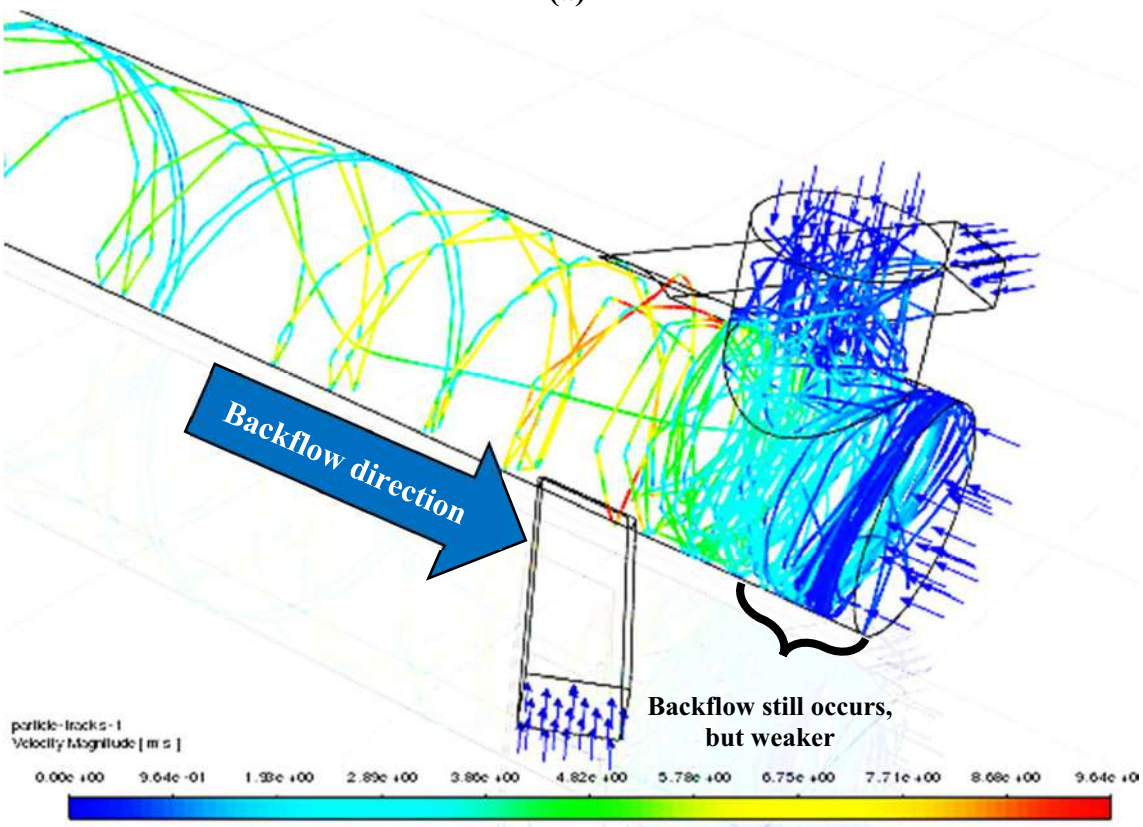

(b)

Fig. 8 Backflow investigation at tangential air pipe of 60° for air flow (**a**), dan rice husk flow (**b**)

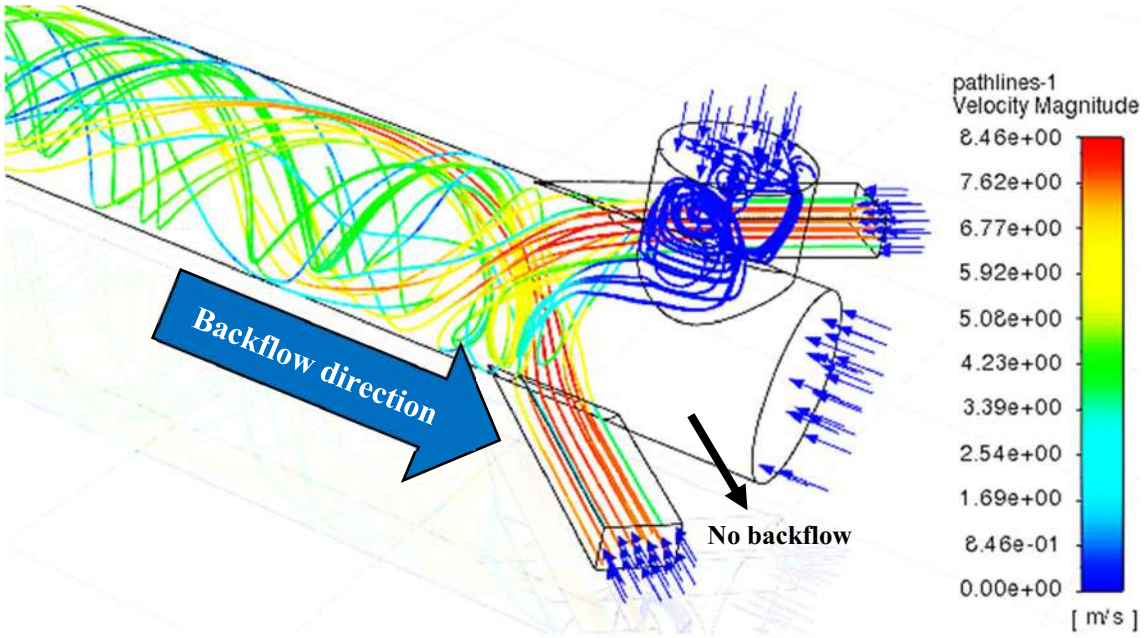

(a)

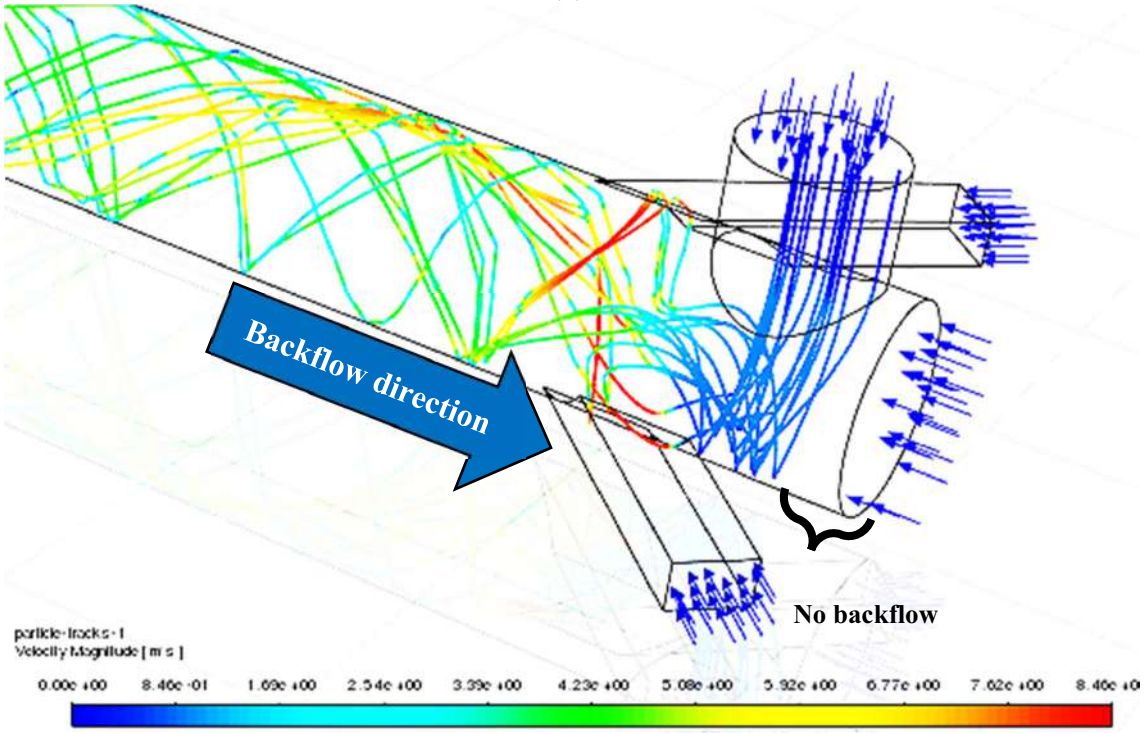

(b)

Fig. 9 Backflow investigation at tangential air pipe of 45° for air flow (**a**), dan rice husk flow (**b**)

and relatively shorter computation time. Moreover, the simulation was validated by a cold test experiment with qualitatively good agreement results.

Supplementary Information The online version contains supplementary material available at https://doi.org/10.1007/s43153-022-00274-y.

Acknowledgements The authors acknowledge the Riset Unggulan PT grants funding, Indonesian Ministry of Research and Technology/National Research and Innovation Agency for the full financial support to this study. Thanks to Mr. Imam Mardhatillah Fajri who has sincerely helped us in manufacturing the suspension furnace 3D design as seen in the Supplementary File. We also greatly thank Akrilik Cipta Jaya (Bandung, Indonesia) for their endeavor to fabricate the acrylic suspension furnace equipped with the cyclone with satisfying results. Finally, a special thank is addressed to Mr. Harben (Biomass Technology Workshop ITB Jatinangor) for his great notion about the acrylic furnace and blower frames as well as his kindness and patient assistance when installing all of the frames.

Declarations

Conflict of interest All authors declare that they have no conflict of interest.

References

ANSYS (2019) ANSYS fluent theory guide 2019 R3. ANSYS Inc

Bhuiyan AA, Naser J (2015) CFD modelling of co-firing of biomass with coal under oxy-fuel combustion in a large scale power plant. Fuel 159:150–168. https://doi.org/10.1016/j.fuel.2015.06.058

Bindar Y (2017) Computational engineering on multidimensional turbulent flows (Rekayasa Komputasi Aliran Turbulen Multidimensi). ITB Press, New York

Bindar Y et al (2022) Large-scale pyrolysis of oil palm frond using two-box chamber pyrolyzer for cleaner biochar production. Biomass Convers Biorefinery. https://doi.org/10.1007/s13399-022-02842-1

Blissett R et al (2017) Valorisation of rice husks using a TORBED® combustion process. Fuel Process Technol 159:247–255. https://doi.org/10.1016/j.fuproc.2017.01.046

Cardoso J et al (2019) Comparative 2D and 3D analysis on the hydrodynamics behaviour during biomass gasification in a pilot-scale fluidized bed reactor. Renew Energy 131:713–729. https://doi.org/10.1016/j.renene.2018.07.080

Chokphoemphun S et al (2019) Rice husk combustion characteristics in a rectangular fluidized-bed combustor with triple pairs of chevron-shaped discrete ribbed walls. Case Stud Therm Eng 14(July):100511. https://doi.org/10.1016/j.csite.2019.100511

Costa JAS, Paranhos CM (2018) Systematic evaluation of amorphous silica production from rice husk ashes. J Clean Prod 192:688–697. https://doi.org/10.1016/j.jclepro.2018.05.028

Defraeye T (2014) Advanced computational modelling for drying processes—a review. Appl Energy 131(Supplement C):323–344

Duan F et al (2013) Experimental study on rice husk combustion in a vortexing fluidized-bed with flue gas recirculation (FGR). Biores Technol 134:204–211. https://doi.org/10.1016/j.biortech.2013.01.125

Fang M et al (2004) Experimental study on rice husk combustion in a circulating fluidized bed. Fuel Process Technol 85(11):1273–1282. https://doi.org/10.1016/j.fuproc.2003.08.002

Fernandes IJ et al (2016) Characterization of rice husk ash produced using different biomass combustion techniques for energy. Fuel 165:351–359. https://doi.org/10.1016/j.fuel.2015.10.086

Gao X et al (2018) CFD modeling of sawdust gasification in a lab-scale entrained flow reactor based on char intrinsic kinetics. Part 1: model development. Chem Eng Process Process Intensif 125(December 2017):280–289. https://doi.org/10.1016/j.cep.2018.02.017

Gomes GMF et al (2016) Rice husk bubbling fluidized bed combustion for amorphous silica synthesis. J Environ Chem Eng 4(2):2278–2290. https://doi.org/10.1016/j.jece.2016.03.049

Guan Y et al (2014) Three-dimensional CFD simulation of hydrodynamics in an interconnected fluidized bed for chemical looping combustion. Powder Technol 268:316–328. https://doi.org/10.1016/j.powtec.2014.08.046

Haider A, Levenspiel O (1989) Drag coefficient and terminal velocity of spherical and nonspherical particles. Powder Technol 58(1):63–70. https://doi.org/10.1016/0032-5910(89)80008-7

Hernowo P et al (2022a) Nature of mathematical model in lignocellulosic biomass pyrolysis process kinetic using volatile state approach. J Taiwan Inst Chem Eng 139:104520. https://doi.org/10.1016/j.jtice.2022.104520

Hernowo P et al (2022b) Chemicals component yield prediction and kinetic parameters determination of oil palm shell pyrolysis through volatile state approach and experimental study. J Anal Appl Pyrol 161:105399. https://doi.org/10.1016/j.jaap.2021.105399

Hoekstra AJ (2000) Gas flow field and collection efficiency of cyclone separators. Dissertation, Technische Universiteit Delft

Hoekstra AJ, Derksen JJ, Van Den Akker HEA (1999) An experimental and numerical study of turbulent swirling flow in gas cyclones. Chem Eng Sci 54:2055–2065. https://doi.org/10.1016/S0009-2509(98)00373-X

Huang Q et al (2010) CFD simulation of hydrodynamics and mass transfer in an internal airlift loop reactor using a steady two-fluid model. Chem Eng Sci 65(20):5527–5536. https://doi.org/10.1016/j.ces.2010.07.021

Kapur PC, Singh R, Srinivasan J (1984) Tube-in-basket burner for rice husk. I: properties of husk as a fuel and basic design considerations. Sadhana 7(4):291–300. https://doi.org/10.1007/BF02811369

Khosravi Nikou MR, Ehsani MR (2008) Turbulence models application on CFD simulation of hydrodynamics, heat and mass transfer in a structured packing. Int Commun Heat Mass Transf 35(9):1211–1219. https://doi.org/10.1016/j.icheatmasstransfer.2008.05.017

Koksal M (2001) Gas mixing and flow dynamics in circulating fluidized beds with secondary air injection. National Library of Canada

Kuprianov VI et al (2010) Combustion and emission characteristics of a swirling fluidized-bed combustor burning moisturized rice husk. Appl Energy 87(9):2899–2906. https://doi.org/10.1016/j.apenergy.2009.09.009

Li Z et al (2019) CFD simulation of a fluidized bed reactor for biomass chemical looping gasification with continuous feedstock. Energy Convers Manag 201(September):112143. https://doi.org/10.1016/j.enconman.2019.112143

Lin CH, Teng JT, Chyang CS (1997) Evaluation of the combustion efficiency and emission of pollutants by coal particles in a vortexing fluidized bed. Combust Flame 110(1–2):163–172

Malekjani N, Jafari SM (2018) Simulation of food drying processes by computational fluid dynamics (CFD): recent advances and approaches. Trends Food Sci Technol 78:206–223. https://doi.org/10.1016/j.tifs.2018.06.006

Malik R et al (2010) Computational fluid dynamics (CFD) based simulated study of multi-phase fluid flow. Defect Diffus Forum 307:1–11. https://doi.org/10.4028/www.scientific.net/DDF.307.1

Mohammed RH et al (2018) Physical properties and adsorption kinetics of silica-gel/water for adsorption chillers. Appl Therm Eng 137:368–376. https://doi.org/10.1016/j.applthermaleng.2018.03.088

Nakhaei M et al (2020) CFD modeling of gas–solid cyclone separators at ambient and elevated temperatures. Processes 8(228):1–26. https://doi.org/10.3390/pr8020228

Nemoda S et al (2005) Experimental and numerical investigation of gaseous fuel combustion in swirl chamber. Int J Heat Mass Transf 48(21–22):4623–4632. https://doi.org/10.1016/j.ijheatmasstransfer.2005.04.004

Norton T, Tiwari B, Sun DW (2013) Computational fluid dynamics in the design and analysis of thermal processes: a review of recent advances. Crit Rev Food Sci Nutr 53(3):251–275

Nunes LJR, Matias JCO, Catalão JPS (2014) Mixed biomass pellets for thermal energy production: a review of combustion models. Appl Energy 127:135–140. https://doi.org/10.1016/j.apenergy.2014.04.042

Panneerselvam R, Savithri S, Surender GD (2009) CFD simulation of hydrodynamics of gas–liquid–solid fluidised bed reactor. Chem Eng Sci 64(6):1119–1135. https://doi.org/10.1016/j.ces.2008.10.052

Panuju DR, Mizuno K, Trisasongko BH (2013) The dynamics of rice production in Indonesia 1961–2009. J Saudi Soc Agric Sci 12(1):27–37. https://doi.org/10.1016/j.jssas.2012.05.002

Park HC, Choi HS (2019) Numerical study of the segregation of pyrolyzed char in a bubbling fluidized bed according to distributor configuration. Powder Technol 355:637–648. https://doi.org/10.1016/j.powtec.2019.07.084

Pashtrapanska M et al (2006) Turbulence measurements in a swirling pipe flow. Exp Fluids 41(5):813–827. https://doi.org/10.1007/s00348-006-0206-x

Pasymi P, Budhi YW, Bindar Y (2017) The effect of inlet aspect ratio (RIA) to the three dimensional mixing characteristics in tangential burner. ARPN J Eng Appl Sci 12(18):5300–5306

Pasymi P, Budhi YW, Bindar Y (2020a) Experimental and numerical investigations of fluid flow behaviors in a biomass cyclone burner. ASEAN J Chem Eng 20(1):88–98. https://doi.org/10.22146/ajche.56708

Pasymi P, Budhi YW, Bindar Y (2020b) Intrinsic parameters of dry chopped miscanthus for cold particle dynamic modeling. J Teknol 82(5):91–100. https://doi.org/10.11113/jt.v82.13534

Prasara AJ, Gheewala SH (2017) Sustainable utilization of rice husk ash from power plants: a review. J Clean Prod 167:1020–1028. https://doi.org/10.1016/j.jclepro.2016.11.042

Ramli Y et al (2022) Simulation study of bamboo leaves valorization to small-scale electricity and bio-silica using ASPEN PLUS. BioEnergy Res. https://doi.org/10.1007/s12155-022-10403-7

Rozainee M (2007) Production of amorphous silica from rice husk in fluidised bed system. Universiti Teknologi Malaysia

Rozainee M et al (2010) Computational fluid dynamics modeling of rice husk combustion in a fluidised bed combustor. Powder Technol 203(2):331–347. https://doi.org/10.1016/j.powtec.2010.05.026

Singh RI, Brink A, Hupa M (2013) CFD modeling to study fluidized bed combustion and gasification. Appl Therm Eng 52(2):585–614. https://doi.org/10.1016/j.applthermaleng.2012.12.017

Steven S et al (2021) Influences of pretreatment, extraction variables, and post treatment on bench-scale rice husk black ash (RHBA) processing to bio-silica. Asia-Pac J Chem Eng 16(5):e2694. https://doi.org/10.1002/apj.2694

Steven S, Restiawaty E et al (2022a) Digitalized turbulent behaviors of air and rice husk flow in a vertical suspension furnace from computational fluid dynamics simulation. Asia-Pac J Chem Eng. https://doi.org/10.1002/apj.2805

Steven S, Friatnasary DL et al (2022b) High cell density submerged membrane photobioreactor (SMPBR) for microalgae cultivation. IOP Conf Ser Earth Environ Sci 963(1):012034. https://doi.org/10.1088/1755-1315/963/1/012034

Steven S, Windari L et al (2022c) Investigation of air and rice husk cold flow structures in the suspension furnace chamber through a simulation study. Int J Thermofluid Sci Technol 9(5):2090501. https://doi.org/10.36963/IJTST.2022090501

Steven S, Hernowo P et al (2022d) Thermodynamics simulation performance of rice husk combustion with a realistic decomposition approach on the devolatilization stage. Waste Biomass Valoriz 13(5):2735–2747. https://doi.org/10.1007/s12649-021-01657-x

Steven S, Restiawaty E, Bindar Y (2022e) Operating variables on production of high purity bio-silica from rice hull ash by extraction process. J Eng Technol Sci 54(3):220304. https://doi.org/10.5614/j.eng.technol.sci.2022.54.3.4

Steven S, Restiawaty E, Bindar Y (2022f) Simple mass transfer simulation using a single-particle heterogeneous reaction approach in rice husk combustion and rice husk ash extraction. IOP Conf Ser Earth Environ Sci 963(1):012050. https://doi.org/10.1088/1755-1315/963/1/012050

Steven, S, Restiawaty, E, et al (2022g) Three-dimensional flow modelling of air and particle in a low-density biomass combustor chamber at various declination angles of tangential and secondary air pipes. Powder Technol 410:117883. https://doi.org/10.1016/j.powtec.2022.117883

Stroh A et al (2015) 3-D numerical simulation for co-firing of torrefied biomass in a pulverized-fired 1 MWth combustion chamber. Energy 85:105–116. https://doi.org/10.1016/j.energy.2015.03.078

Suranani S, Goli VR (2012) Modeling fluidized bed combustion of rice husk. Int Conf Chem Civil Environ Eng 2012:305–308

Sylvia N et al (2019) A computational fluid dynamic comparative study on CO_2 adsorption performance using activated carbon and zeolite in a fixed bed reactor. IOP Conf Ser Mater Sci Eng 536(1):012042. https://doi.org/10.1088/1757-899X/536/1/012042

Wang T et al (2019) Combustion behavior of refuse-derived fuel produced from sewage sludge and rice husk/wood sawdust using thermogravimetric and mass spectrometric analyses. J Clean Prod 222(2019):1–11. https://doi.org/10.1016/j.jclepro.2019.03.016

Werther J et al (2000) Combustion of agricultural residues. Prog Energy Combust Sci 26(1):1–27. https://doi.org/10.1016/S0360-1285(99)00005-2

Yang S et al (2019) Eulerian–Lagrangian simulation of air-steam biomass gasification in a three-dimensional bubbling fluidized gasifier. Energy 181:1075–1093. https://doi.org/10.1016/j.energy.2019.06.003

Yang S et al (2020) Particle-scale characteristics of the three distinct regions in the multi-chamber slot-rectangular spouted bed. Powder Technol 360:658–672. https://doi.org/10.1016/j.powtec.2019.10.038